The effect of silica mass ratio on pore structure and magnetic characteristics of Fe_3O_4@SiO_2 core-shell nanoparticles

Munasir Nasir[1,*], Lydia Rohmawati[1], Nuhaa Faizatunnisa[2], Ahmad Taufiq[3]

[1]Department of Physics, Faculty of Mathematics and Sciences, Universitas Negeri Surabaya (Unesa), Surabaya-Indonesia
[2]Department of Chemistry, FSAD, Institut Teknologi Sepuluh Nopember (ITS), Surabaya-Indonesia
[3]Department of Physics, Universitas Negeri Malang (UM), Malang-Indonesia

[*]*Corresponding author: Tel. :+6285850493870*
E-mail: munasir_physics@unesa.ac.id (Munasir Nasir)

Received: 06 February 2023
Revised: 07 October 2023
Accepted: 06 January 2024

Abstract

The fabrication of Fe_3O_4@SiO_2 core-shell was prepared from natural iron sand as Fe_3O_4 core resource and in situ SiO_2-coating method. The Fe_3O_4@SiO_2 was synthesized via an ultrasonic route with various ratios of tetraethyl orthosilicate (TEOS) to evaluate the core-shell's morphological, pore structure, and magnetic properties. XRD and FTIR were used to characterize the prepared Fe_3O_4 and Fe_3O_4@SiO_2. SEM analyzed the effect of the TEOS on the particle size, and TEM observed the morphology of core-shell and shell thickness. The BET data revealed that Fe_3O_4@SiO_2(65) exhibited a larger diameter pore size of 88.17 nm and eight times higher BET surface area (80.23 m^2/g) than Fe_3O_4@SiO_2(55) and Fe_3O_4@SiO_2(45) (27.69 nm; 10.5 m^2/g). The VSM data indicated that the more TEOS addition on Fe_3O_4@SiO_2 caused the decrease of magnetization value but still gave good magnetic properties from 95.32 emu/g for Fe_3O_4@SiO_2(45) to 17.02 emu/g for Fe_3O_4@SiO_2(65). The study found that the higher content of SiO_2 reduced the agglomeration of the Fe_3O_4 core indicated by no hysteresis loop on the N_2 adsorption-desorption curve of Fe_3O_4@SiO_2(65), resulting in core-shell material with better properties in higher specific surface area, average pore size and volume for further application.

Keywords: Fe_3O_4@SiO_2 Core-Shell, Nanoparticles, TEOS, Magnetic Nanoparticle

Introduction

Recently, Fe_3O_4 nanoparticles have provided unique material properties and have a significant role in various applications due to their essential superparamagnetic properties, which show high saturation magnetization but remnant magnetism and low coercivity[1]. For example, the Fe_3O_4 magnetic feature eases the separation of material from the mixed system, such as for the adsorption application[2], catalyst in the reaction[3], and drug delivery system[4]. Indonesia has abundant iron sand that can be used as a Fe_3O_4 source. This iron sand has been reported to produce Fe_3O_4, replacing the Fe_3O_4 synthetics route from expensive $FeCl_3$ material [5,6]. Many research attempts are related to studying chemical stability, structure, magnetic properties, and synthesis methods to support its Fe_3O_4 magnetic application[7,8]. The problem with using Fe_3O_4 in the direct application is that it is chemically unstable due to the high surface energy of Fe_3O_4 nanoparticles, causing particle agglomeration[9]. One of the most effective methods to cope with the problem is to incorporate/combine amorphous silica material with Fe_3O_4 NPs. Amorphous mesoporous silica material has a non-toxic nature, a highly specific surface, an ordered mesoporous structure, tunable pore size, and volumes with abundant Si-OH bonds on the pore surface[10].

Core-shell nanomaterials with magnetic Fe_3O_4 nanoparticles as the core have been successfully synthesized previously, such as Fe_3O_4@TiO_2[11], Fe_3O_4@Ag[12], and Fe_3O_4@ZnO[13] using hydrothermal techniques; Fe_3O_4@SiO_2 was carried out using the Stöber method[14]. The core-shell nanoparticles showed superparamagnetic behavior at room temperature, and their toxicity was evaluated using hepatocellular carcinoma liver tumor cells. Furthermore, it has potential applications in biomedical and pharmaceutical fields thanks to its excellent properties, such as increased thermal and chemical stability, dispersibility, low toxicity [6,15], pH-responsive drug release, and biocompatibility[15,16]. Core-shell Fe_3O_4@SiO_2 and its modification with Ag doping, Fe_3O_4@SiO_2-Ag is very effective as an anti-bacterial agent (E. Coli and S. Aureus) and an anticancer drug carrier[17], also helpful in designing thermal seeds in magnetic hyperthermia therapy[18], and for environmental applications[15–22].

Modifications of the Fe_3O_4 magnetic surface with SiO_2 enable selective targeting by forming functional groups on the surface through chemical bonds (covalent, ionic, or hydrogen). Due to their hydrophilic properties, this silica coating feature possesses excellent dispersibility and chemical stability in aqueous solutions[23] . However, the fabrication of Fe_3O_4@SiO_2 core-shell is still challenging due to the aggregation of multiple Fe_3O_4 magnets during surface coating. The aggregation of the Fe_3O_4 core

impacts the decrease of the surface area and limits their applications, such as in adsorption and bio immobilization[24]. $Fe_3O_4@SiO_2$, as a drug carrier or adsorbent, needs a high surface-to-volume (S/V) ratio, which can lead to more robustness in their application[25,26]. The surface-to-volume ratio of nanomaterial plays a vital role because the high S/V increases the biomolecule or dye molecule density that can be adsorbed in the $Fe_3O_4@SiO_2$ surface[27]. Therefore, the additional silica ratio and the thickness of the silica shell on the $Fe_3O_4@SiO_2$ significantly affect the aggregation of Fe_3O_4, the pore structure, and the characteristics of the core shell[26,28]. The Fe_3O_4 with uniform and controlled thickness silica coating is still being challenged. Therefore, adjusting silica content is needed to tailor the end properties of the material.

In this study, we report the facile synthesis of $Fe_3O_4@SiO_2$ with the in-situ method. The Fe_3O_4 core was prepared from iron sand by the co-precipitation method. The incorporation of SiO_2 to Fe_3O_4 was adjusted according to the silica ratio on the $Fe_3O_4@SiO_2$. Silica coating parameters are used to tune this silica layer's thickness and minimize the Fe_3O_4 particle agglomeration. The magnetic incorporation of SiO_2 into Fe_3O_4 is tailored to particle size, pore, surface area, and magnetic properties, which are discussed in this paper. By adjusting the silica ratio on the $Fe_3O_4@SiO_2$, the thickness of the $Fe_3O_4@SiO_2$ shell can be controlled and significantly impact the increment of the core shell's surface area and pore diameter. This feature of silica microspheres with magnetic properties is an available prospect for the wide potential application of iron sand as raw material for better uses.

Materials and methods

2.1. Materials

All chemicals were in analytical grade and used without any further purification. Iron sand (98% Fe_3O_4), hydrochloric acid (HCl, Pro Analysis (37%)), ammonium hydroxide (NH_4OH), ethanol (C_2H_5OH, 96%), ammonia ($NH_3.H_2O$,25%), tetraethyl orthosilicate (TEOS, 97%) were purchased from Sigma Aldrich, distilled water, and filter paper (Whatman, 60mm).

2.2. Synthesis Method

2.2.1. Synthesis of Fe_3O_4 Magnetic

The synthesis of Fe_3O_4 nanoparticles was prepared and extracted from iron sand using the co-precipitation method, as done in the previous research[29]. A mass of 20 g of iron sand was dissolved in

38 mL of HCl (2M) and stirred for 10-12 min at 60 °C. When the color changed to yellow, 24 mL of NH_4OH (6M) was added and stirred until the color became dark black. The solution was separated and washed with distilled water several times. The Fe_3O_4 was dried in an oven at 70 °C for 12 h. The chemical reaction proceeds as follows [16–18] :

$$Fe_3O_{4(s)} + 8HCl_{(l)} \rightarrow 2FeCl_{3(l)} + FeCl_{2(l)} + 4H_2O_{(l)} \quad (1)$$

$$2FeCl_{3(l)} + FeCl_{2(l)} + 8NH_4OH.H_2O_{(l)} \rightarrow Fe_3O_{4(s)} + 8NH_4Cl_{(l)} + 5H_2O_{(l)} \quad (2)$$

2.2.2. Synthesis of Fe_3O_4@SiO_2 Core-Shell

The synthesis process of Fe_3O_4@SiO_2 core-shell was carried out using the in-situ coating method as done according to previous reports with a little change[19]. A mass of 1 g of Fe_3O_4 nanoparticle powder was mixed with 24 mL distilled water and dispersed in ultra-sonification for 30 min. Furthermore, 240 mL of ethanol was added to the mixture while stirring until it was interpreted as evenly mixed. Next, 4 mL of ammonia and a variation of mass ratio TEOS addition (4.5, 5.5, and 6.5 mL) were added. The mass variation of TEOS addition in Fe_3O_4 were subsequently denoted as Fe_3O_4@SiO_2(45), as Fe_3O_4@SiO_2(55), and as Fe_3O_4@SiO_2(65). The mixture was stirred for eight hours at room temperature. The resulting solution was brownish-black and washed with distilled water until it reached a pH of 7. The final stage of the resulting precipitate was dried at 60°C for 24 h; these are the chemical reactions of the prepared SiO_2 shell from TEOS:

$$Si(OC_2H_5)_{4(aq)} + 4H_2O_{(l)} \rightarrow Si(OH)_{4(s)} + 4C_2H_5OH_{(g)} \quad (3)$$

$$Si(OH)_{4(s)} + Si(OH)_{4(s)} \rightarrow (OH)_3Si - O - Si(OH)_{3(s)} + H_2O_{(l)} \quad (4)$$

2.2.3. Mechanism of Fe_3O_4@SiO_2 core-shell formation

Figure 1 shows the mechanism for the formation of core-shell Fe_3O4@SiO_2. Tetraethyl orthosilicate (TEOS) was used as a silica precursor to make a SiO_2 layer on the surface of Fe_3O_4 nanoparticles. This reaction proceeds through hydrolysis and condensation reaction through the ionization of $Si(OC_2H_5)_4$. $Si(OC_2H_5)_4$ reacts with H_2O and is converted through ionization to form orthosilicic acid $Si(OH)_4$, which can be used as a silicon oxide precursor and ethanol gas (C_2H_5OH). The orthosilicic acid formed binds to the OH group on the surface of the Fe_3O_4 nanoparticles, and the condensation reaction is then repeated to form a SiO_2 layer while forming a network structure around the particles. The dense silica coating factors affecting the mesoporous shell formation are ethanol and ammonia concentrations.

The modification of the surface of Fe_3O_4 nanoparticles can be conducted with appropriate ligands or functional groups. This modification is believed to increase its stability and prevent agglomeration. Silane coupling agents, for example, can be used to modify the surface chemistry of Fe_3O_4 nanoparticles. The use of ultrasonication or other dispersion techniques during the synthesis process is to break up lumps. However, be careful in increasing the temperature during ultrasonication, as excessive heat can cause further caking. Optimizing the strength and duration of ultrasonication and mechanical stirring during ultrasonication can help distribute the heat generated by ultrasonication and prevent local overheating.

2.3. Characterizations

All materials preparation was characterized by X-ray diffraction (Paan Analytical, Type: Expert Pro) and scanned at a range of 5°-75°. Fourier Transform infrared spectroscopy (FTIR, Shimadzu, Tipe: IRPrestige) analyzed functional groups at 400 to 4000 cm^{-1} wavenumbers. The material morphological structure and particle size were conducted using scanning electron microscopy (SEM, Zeiss Evo MA 10), and the formation of the core-shell structure was monitored using a transmission electron microscope (TEM) (Hitachi HT7700, USA). The magnetic properties were recorded at room temperature using a vibrating sample magnetometer (VSM; 7404, Lakeshore, USA).

Results and discussion

3.1 Structure Analysis of $Fe_3O_4@SiO_2$ magnetic

The XRD patterns of Fe_3O_4, TEOS, and $Fe_3O_4@SiO_2$ with different amounts of TEOS are shown in **Figure 2**. In all synthesized $Fe_3O_4@SiO_2$ core-shell, five major 2θ diffraction peaks at 30.2°, 35.5°, 43.1°, 57.1°, and 62.8° observed, which represent (220), (311), (400), (422) and (511) planes of standard Fe_3O_4 magnetic pattern, respectively[29]. The characteristic of amorphous silica SiO_2 was showed in broad diffraction peak at 24°. This peak of silica is weak in all synthesized materials, which might be due to a small signal-to-noise ratio[5]. The obtained $Fe_3O_4@SiO_2$ XRD patterns showed that the addition of SiO_2 did not significantly change the structure of Fe_3O_4 and revealed that after coating silica, the core still persevered its crystallinity. Furthermore, as the loading amount of SiO_2 increased, the intensity peat at 35.5° was decreased, revealing the reduction of Fe_3O_4 crystallinity. In addition, the peak width at 35° of all synthesized material is broader than that of Fe_3O_4 magnetic. This is because the Fe_3O_4 magnetic surface was under stress between the Fe_3O_4 core and SiO_2 shell due to the slight increment of inter-planar distance[10]. The crystallite size of the Fe_3O_4 cores calculated by the Debye Scherrer equation reveals 1.6 nm while the $Fe_3O_4@SiO_2$(45), $Fe_3O_4@SiO_2$(55), $Fe_3O_4@SiO_2$(65) have 8.47, 14.12, and 22.59 nm, respectively. These results reveal that adding silica content increased the crystallite size of the $Fe_3O_4@SiO_2$. This examination of XRD results verifies that the $Fe_3O_4@SiO_2$ are constructed of Fe_3O_4 and SiO_2 (shown in **Table 1**) [30–32].

3.3. Functional Analysis by FTIR of Fe_3O_4@SiO_2 magnetic

The characterization of the synthesized Fe_3O_4@SiO_2 core-shell with mass ratio variation of SiO_2 is obtained through the FTIR spectrum, represented in **Figure 3**. The Fe_3O_4 magnetic have adsorption characteristic peaks at 582 and 456 cm^{-1} assigned to the stretching vibration of Fe in the tetrahedral and octahedral region[30], in which these peaks also appear in the magnetic nanoparticles spectrums after TEOS addition. The FTIR spectrum of TEOS showed the adsorption band of Si-O-Si asymmetric vibration, Si-O stretching vibration, and Si-O-Si symmetric at 1130, 960, and 800 cm^{-1}, respectively[28,32]. This absorption peak is present in all synthesized Fe_3O_4@SiO_2 core-shell materials, and Si-O-Si asymmetric vibration intensity increases with increasing silica ratio (TEOS) of Fe_3O_4 magnetic particles. Moreover, the silanol group (Si-OH) on the surface of SiO_2 at 1629 cm^{-1}[14] is present in all synthesized materials. This confirms that the raw material's functional groups and chemical bondings indicate that the SiO_2 (the shell) was successfully incorporated in Fe_3O_4 (the core).

The remanent magnetization (Mr), field coercivity (Hc), and saturation (Ms) data obtained by the magnetic hysteresis loop are essential in determining the magnetic properties of the material. The saturation magnetic is a state when the maximal of the external magnetic field can be applied to the material. The coercivity is a magnetic field described as material's resistance to make zero magnetism. This coercivity value determined the nature of paramagnetic. The higher Hc value indicates stronger paramagnetic nature properties[33]. The remanent magnetization is the magnetization residue after removing the external magnetic field. **Table 2** compares the magnetic properties of the Fe_3O_4 and Fe_3O_4 after TEOS coating. Fe_3O_4 has the highest Hc value, 0.067 tesla, which exhibited a superparamagnetic nature. The addition of TEOS contributes to lowering the Hc and remanent values along with the larger crystal size obtained by the Debye Scherrer formula from XRD data. A detailed investigation by Li et al. for Fe_3O_4 NPs envisages a decrease of both remanent magnetization and coercivity with an increase in size even when the saturation magnetization increases[34]. This data revealed that the smaller crystal size tended to have a higher value of Hc and Mr. The coercivity field was further discussed in **Figure 4**. The coercive field of Fe_3O_4 was smaller than the others. Fe_3O_4@SiO_2(45) has a coercivity field similar to Fe_3O_4. After the addition of more TEOS content on the Fe_3O_4, the coercivity became larger. By designing the Fe_3O_4@SiO_2 core-shell structure, the Fe_3O_4 core acts as a soft magnetic (weak magnetic anisotropy which easily magnetized and demagnetized), and the SiO_2 acts as the shell of a hard magnetic (large magnetic anisotropy)[35]. The Ms value, obtained by applying the law of approach to saturation[36], increases with increasing crystal size for all samples. Meanwhile, Hc and remanent magnetization (Mr) are also affected by crystallite size. The high Hc value may be caused by the strong spin interactions in the highly crystalline Fe_3O_4 NPs during spin alignment. The crystalline properties of Fe_3O_4 NPs affect their magnetic properties, especially Hc. This trend is consistent with that found in the previous work38.

In **Figure 5**, the results of the measurements of the hysteresis curve for the sample Fe_3O_4@SiO_2 core-shell, prepared by the in-situ method, show a trend of decreasing magnetization value with the

addition of layers of SiO_2 particle as a covering for the Fe_3O_4 particles. The magnetization saturation values of Fe_3O_4, Fe_3O_4@SiO_2 (45, 55, and 65) were 95.32, 80.58, 23.62, and 17.02 emu/g [29][37]. The magnitude of magnetization decreased from approximately 95.32 emu/g to 17.02 emu/g, along with an increase in the ratio mass of TEOS (46, 55, and 65) (see **Figure 5a** (b-d)), and the shell thicknesses increased from 142 to 161 nm.

3.5. Morphology of Fe_3O_4@SiO_2 magnetic

The morphology of Fe_3O_4@SiO_2 with different Silica ratios was investigated by SEM image. **Figure 6** shows the spherical-like morphology of both synthesized Fe_3O_4@SiO_2 materials. The Fe_3O_4@SiO_2 with an addition ratio of 45 of TEOS has a slightly rough surface, whereas the surface of the Fe_3O_4@SiO_2 with an addition ratio of 65 of TEOS appears to be relatively smooth. The TEM images of Fe_3O_4 and synthesized Fe_3O_4@SiO_2 are presented in **Figure 7**. The Fe_3O_4 nanoparticles have spherical shapes and showed an increment of particle size after coating with SiO_2. The particle size was estimated at 150 nm and 161 nm for Fe_3O_4@SiO_2(45) and Fe_3O_4@SiO_2(65). Meanwhile, the Fe3O4, before coating, has an estimated particle size of 120 nm. Meanwhile, the average particle size observed from SEM and TEM indicates the size of the Fe_3O_4 NPs. The size of the Fe_3O_4 core we obtained exceeds 100 nm because it is probably caused by the Fe_3O_4 NPs synthesis method we used. As reported, the formation of Fe_3O_4 follows the nucleation growth mechanism via the oxidation-precipitation method. Nucleation of magnetite particles occurs when the molar ratio of $Fe(OH)_2$/$Fe(OH)_3$ approaches 1:2, a characteristic value of magnetite structure. Then, Fe_3O_4 nuclei begin to grow. Therefore, the product size highly depends on reaction conditions such as reaction time, molar ratio of $FeSO_4$ and oxidizing agent, and concentration of $FeSO_4$, etc. [21,38]

From the TEM image, it can be seen that the core-shell formation is identified by two different contrasts observed: the dark contras of the Fe_3O_4 core and the light contrast of the SiO_2 shell. The layer of SiO_2 was estimated to be around 3 nm for Fe_3O_4@SiO_2(45) and 6 nm for Fe_3O_4@SiO_2(65). The existence of SiO_2 in Fe_3O_4 aligns with previous FTIR and XRD results. Furthermore, this SEM and TEM result showed that the additional SiO_2 ratio exhibits different layers, surface roughness, and particle size. The more TEOS addition results in a thicker and smoother layer of SiO_2 and larger particles of Fe_3O_4@SiO_2 [39,40].

The more TEOS addition results in a thicker and smoother layer of SiO_2 and larger particles of Fe_3O_4@SiO_2[9]. TEOS acts as a silica layer maker on the Fe_3O_4@SiO_2. It started from the corporation of the SiO_2 layer via Fe-O-Si chemical bonding on the surface Fe_3O_4. The addition of TEOS subsequently will construct Si-O-Si silica chain polymers that grow layer by layer, corresponding to shell thickness increment of Fe_3O_4@SiO_2. These chemical bonds were identified in previous FTIR data. Adding TEOS to Fe_3O_4 contributes to the size increment of nanoparticles and the core shell. This finding also aligns with the research result of Prado et al., (2012)[35] , which revealed that the higher TEOS/Fe_3O_4 molar ratio would lead to a thicker silica shell.

The Fe_3O_4 nanoparticles obtained by co-precipitation due to the large surface-to-volume ratio, high surface energy, and magnetic dipole-dipole attractions between the particles, and magnetic nanostructures

are highly prone to aggregation. Therefore, controlling the core size is necessary by choosing the correct method, solvent, and precursor to obtain the desired core size. To synthesize well-dispersed silica-coated Fe_3O_4 NPs, the sol–gel method, the Stöber method, and microemulsion are the most common methods for coating the surface of Fe_3O_4 nanoparticles with silica. Silica coating on the surface of Fe_3O_4 with various layers cannot completely change the size of the morphology formed.

EDX analysis results obtained for Fe_3O_4@SiO_2-core-shell showed that the elemental composition of Si and Fe with the corresponding mass percentage of 4.0% and 51.0% (Fe_3O_4@SiO_2(45)) then 26.0% and 28.0% (Fe_3O_4@SiO_2(65)), respectively. The elemental mapping (**Figure 8**) of Fe_3O_4@SiO_2-core-shell morphology shows that Si is more dominant on the surface than Fe with an increase in the ratio mass of TEOS. This indicates the successful preparation of Fe_3O_4@SiO_2-core-shell in the ratio mass of TEOS, as evidenced by other characterizations.

3.6. N_2 Adsorption-desorption of Fe_3O_4@SiO_2 magnetic

The type of porous structure of synthesized Fe_3O_4@SiO_2 was further analyzed by the N_2 adsorption-desorption experiment in **Figure 9** and summarized in **Table 3**. The hysteresis loop of obtained synthesized material was classified as a type IV pattern for all materials microspheres, which show mesoporous characteristics[40]. The isotherm of Fe_3O_4 with a lower Si amount (ratio 45) showed a notable hysteresis loop in the relative pressure range of 0.3-0.9, which indicates the mesopores formation due to agglomeration[41]. Furthermore, the agglomeration of Fe_3O_4@SiO_2 with lower Si content caused the smaller specific surface area, average pore size, and volume. It can be seen that the histogram of the Fe_3O_4@SiO_2 composite with Si content between the two other materials has a pattern that is almost similar to 45. The average pore diameter of Fe_3O_4@SiO_2(45), Fe_3O_4@SiO_2(55) , and Fe_3O_4@SiO_2(65) were 27.69, 33.04, and 88.17 nm, respectively. In addition, the Fe_3O_4 with a ratio of 65 of TEOS addition has a BET surface area of 80.23 m^2/g, which is eight times higher than the Fe_3O_4 with a ratio of 45 of TEOS addition (10.5 m^2/g). Interestingly, from **Figure 9,** it was seen that Fe_3O_4 with a higher Si amount (ratio 65) has no hysteresis loop. This result indicates that more content of the SiO_2 layer helps reduce the agglomeration, which releases the void space among particles and reflects in higher specific surface area, average pore size, and volume.

The porosity analysis was done by simulating the adsorption curve using density functional theory (DFT). The obtained porosity curve is shown in **Figure 10**. Fe_3O_4@SiO_2(45) has a pores size of 27.691 Å (2.7691 nm), Fe_3O_4@SiO_2(55) has a pores size of 33.041 Å (3.3041nm), and Fe_3O_4@SiO_2(65) is 88.171 Å (8.8171 nm). The results indicated that adding SiO_2 to the surface of the Fe_3O_4 nanoparticles would make the pores more mesoporous.

In the core-shell synthesis, Fe_3O_4@SiO_2 may be linked to Janus nanofluids through the formation of a unique nanoparticle structure that combines the different properties of the core (Fe_3O_4 nanoparticles) and the shell (SiO_2) [42]. The agglomeration process of core-shell particles with TEOS precursor media can be related to nanofluids, and it can be considered whether the core-shell structure influences the agglomeration of these particles and the morphology of the aggregates formed [42,43].

For further studies, the influence of aggregation morphology on thermal conductivity provides a basis for understanding how Janus nanofluid aggregates are structured, which may be influenced by core-shell synthesis. Moreover, the image analysis modeling approach on Janus nanofluids can provide a deep understanding of particle morphology. It is necessary to consider whether this modeling approach can be applied to nanofluids resulting from core-shell synthesis to describe and predict the distribution of particle morphology in more detail [42–45].

Conclusions

This research successfully synthesized the Fe_3O_4@SiO_2 core-shell from natural iron sand using the in-situ SiO_2 coating method. The silica thickness ranging from 3 to 6 nm could be controlled by changing the TEOS mass ratio from 5.5 mL to 6.5 mL. The surface area tended to follow the same pattern as the thickness increased. Increasing the percentage of TEOS resulted in an increase in surface area and a decrease in magnetization of Fe_3O_4@SiO_2. The study found that adding TEOS content (SiO_2) reduced the agglomeration of Fe_3O_4-core. This Fe_3O_4@SiO_2 magnetic material with higher specific surface area, average pore size, volume, and good magnetic properties could make promising materials for further application.

Acknowledgments

The authors would like to thank the State University of Surabaya, especially the Department of Physics, for allowing the use of laboratory facilities and LPPM-UNESA, which provided grants through competitive research (PDKN-DRTPM), with the contract number: B/29525/UN38.III.1/ LK.04.00/ 2023.

Abbreviations

SiO_2 : Silicon dioxide (or silica)
Fe_3O_4 : Iron (II) oxide or magnetite
NPs : Nanoparticles
TEOS : Tetraethyl orthosilicate
XRD : X-Ray diffraction
FTIR : Fourier Transform Infra-Red
Mr : Remanent magnetic field
Hc : Coercivity magnetic field
Ms : Saturation magnetic field
VSM : Vibrating sample magnetometer
EDX : Energy Dispersive X-ray
SEM : Scanning Electron Microscope
TEM : Transmission Electron Microscopy
nm : Nanometer
BET : Brunauer-Emmett-Teller
S_{BET} : Specific surface area (of porous material by BET method)
VSM : Vibrating sample magnetometer

N_2 : Gas of Nitrogen
DFT : Density functional theory
D : Crystal size (by Debye Scherrer formula)
β : full width at half maximum of peak X-ray diffraction
λ : X-ray wavelength (Cu K_α)
Å : Angstrom (1 Å = 10^{-10} meter = 10 nm)

References

1. Patsula, V., Kosinová, L., Lovrić, M., et al., "Superparamagnetic Fe_3O_4 Nanoparticles: Synthesis by Thermal Decomposition of Iron(III) Glucuronate and Application in Magnetic Resonance Imaging", *ACS Appl. Mater. Interfaces*, **8**(11), pp. 7238–7247 (2016).
2. Pant, B., Ojha, G. P., Kim, H. Y., et al., "Fly-ash-incorporated electrospun zinc oxide nanofibers: Potential material for environmental remediation", *Environ. Pollut.*, **245**, pp. 163–172 (2019).
3. Yue, Q., Liu, C., Wan, Y., et al., "Defect engineering of mesoporous nickel ferrite and its application for highly enhanced water oxidation catalysis", *J. Catal.*, **358**, pp. 1–7 (2018).
4. Kandasamy, G., Soni, S., Sushmita, K., et al., "One-step synthesis of hydrophilic functionalized and cytocompatible superparamagnetic iron oxide nanoparticles (SPIONs) based aqueous ferrofluids for biomedical applications", *J. Mol. Liq.*, **274**, pp. 653–663 (2019).
5. Rahmawati, R., Taufiq, A., Sunaryono, S., et al., "Synthesis of Magnetite (Fe_3O_4) Nanoparticles from Iron sands by Coprecipitation-Ultrasonic Irradiation Methods", *J. Mater. Environ. Sci.*, **9**(1), pp. 155–160 (2018).
6. Nikmah, A., Taufiq, A., and Hidayat, A., "Synthesis and Characterization of Fe_3O_4/SiO_2 nanocomposites", *IOP Conf. Ser. Earth Environ. Sci.*, **276**(1) (2019).
7. A. Taufiq, Sunaryono, E. G. R. Putra, S. Pratapa, and D., "Nano-structural studies on Fe_3O_4 particles dispersing in a magnetic fluid using x-ray diffractometry and small-angle neutron scattering", *Mater. Sci. Forum*, **827**, pp. 213–218 (2015).
8. Grebennikov, I. S., Savchenko, A. G., Zaytseva, M. P., et al., "Structure and Magnetic Properties of Nanopowders of Iron Oxides and Hybrid Nanopowders of the Core–Shell Type Based on Them", *Bull. Russ. Acad. Sci. Phys.*, **82**(9), pp. 1222–1231 (2018).
9. Zeng, H., Li, J., Liu, J. P., et al., "Exchange-coupled nanocomposite magnets by nanoparticle self-assembly", *Nature*, **420**(6914), pp. 395–398 (2002).
10. Cha, J. H., Choi, H. H., Jung, Y. G., et al., "Novel synthesis of core–shell structured $Fe_3O_4@SiO_2$ nanoparticles via sodium silicate", *Ceram. Int.*, **46**(10), pp. 14384–14390 (2020).
11. Madhubala, V., Nagarajan, C., Baskaran, P., et al., "Formulation of magnetic core-shell nanostructured $Fe_3O_4@TiO_2$ for cytotoxic activity against Huh-7 cells", *Inorg. Chem. Commun.*, **149**,110430 (2023).
12. Madhubala, V., Nagarajan, C., Baskaran, P., et al., "Influences of superparamagnetic Fe_3O_4@Ag core-shell nanoparticles on the growth inhibition of Huh-7 cells", *Mater. Today Commun.*, **35**,106139 (2023).
13. Madhubala, V. and Kalaivani, T., "Phyto and hydrothermal synthesis of Fe_3O_4@ZnO core-shell nanoparticles using Azadirachta indica and its cytotoxicity studies", *Appl. Surf. Sci.*, **449**, pp. 584–590 (2018).
14. Khalid, A., Ahmed, R. M., Taha, M., et al., "Fe_3O_4 nanoparticles and $Fe_3O_4@SiO_2$ core-shell: synthesize, structural, morphological, linear, and nonlinear optical properties", *J. Alloys Compd.*, **947**, 169639 (2023).
15. Cai, W., Guo, M., Weng, X., et al., "Modified green synthesis of $Fe_3O_4@SiO_2$ nanoparticles for pH responsive drug release", *Mater. Sci. Eng. C*, **112**(2020).
16. García, L., Garaio, E., López-Ortega, A., et al., "Fe_3O_4-SiO_2 Mesoporous Core/Shell Nanoparticles for Magnetic Field-Induced Ibuprofen-Controlled Release", *Langmuir*, **39**(1) (2022).
17. Romdoni, Y., Kadja, G. T. M., Kitamoto, Y., et al., "Synthesis of multifunctional $Fe_3O_4@SiO_2$-Ag nanocomposite for antibacterial and anticancer drug delivery", *Appl. Surf. Sci.*, **610**, 155610 (2023).
18. Goswami, P., Mathur, J., and Srivastava, N., "Silica nanoparticles as novel sustainable approach for plant growth and crop protection", *Heliyon*, **8**(7), p. e09908 (2022).
19. Alterary, S. S. and Alkhamees, A., "Synthesis, surface modification, and characterization of

Fe_3O_4@SiO_2core@shell nanostructure", *Green Process. Synth.*, **10**(1), pp. 384–391 (2021).
20. Lajevardi, A., Hossaini Sadr, M., Badiei, A., et al., "Synthesis and characterization of Fe_3O_4@SiO_2@MIL-100(Fe) nanocomposite: A nanocarrier for loading and release of celecoxib", *J. Mol. Liq.*, **307**, p. 112996 (2020).
21. Lei, Y., Zhang, X., Meng, X., et al., "The preparation of core–shell Fe_3O_4@SiO_2 magnetic nanoparticles with different surface carboxyl densities and their application in the removal of methylene blue", *Inorg. Chem. Commun.*, **139**(December 2021), p. 109381 (2022).
22. Taufiq, A., Munasir, Teraningtyas, A., et al., "Nanosized Fe_3O_4/SiO_2 core-shells fabricated from natural sands, magnetic properties, and their application for dye adsorption", *Eng. Appl. Sci. Res.*, **49**(3), pp. 340–352 (2022).
23. Hui, C., Shen, C., Tian, J., et al., "Core-shell Fe_3O_4@SiO_2 nanoparticles synthesized with well-dispersed hydrophilic Fe3O4 seeds", *Nanoscale*, **3**(2), pp. 701–705 (2011).
24. Samadi, M. S., Shokrollahi, H., and Zamanian, A., "The magnetic-field-assisted synthesis of the Co-ferrite nanoparticles via reverse co-precipitation and their magnetic and structural properties", *Mater. Chem. Phys.*, **215**, pp. 355–359 (2018).
25. Taylor, K. M. L., Kim, J. S., Rieter, W. J., et al., "Mesoporous silica nanospheres as highly efficient MRI contrast agents", *J. Am. Chem. Soc.*, **130**(7), pp. 2154–2155 (2008).
26. Vogt, C., Toprak, M. S., Muhammed, M., et al., "High quality and tuneable silica shell-magnetic core nanoparticles", *J. Nanoparticle Res.*, **12**(4), pp. 1137–1147 (2010).
27. Abbas, M., Takahashi, M., and Kim, C., "Facile sonochemical synthesis of high-moment magnetite (Fe_3O_4) nanocube", *J. Nanoparticle Res.*, **15**(1) (2013).
28. Taib, N. I., Woodward, R. C., and Pierre, T. G. S., "The Effect of Silica Shell Thickness on Magnetic and Proton Relaxometric Properties: Fe_3O_4@mSiO_2 Nanoparticles", *IEEE Trans. Magn.*, **58**(2), pp. 1–7 (2022).
29. Munasir, N., Kusumawati, R. P., Kusumawati, D. H., et al., "Characterization of Fe_3O_4/rGO composites from natural sources: Application for dyes color degradation in aqueous solution", *Int. J. Eng. Trans. A Basics*, **33**(1), pp. 18–27 (2020).
30. Almessiere, M. A., Slimani, Y., Güner, S., et al., "Magnetic and structural characterization of Nb^{3+} -substituted $CoFe_2O_4$ nanoparticles", *Ceram. Int.*, **45**(7), pp. 8222–8232 (2019).
31. Wo, R., Li, Q. L., Zhu, C., et al., "Preparation and Characterization of Functionalized Metal-Organic Frameworks with Core/Shell Magnetic Particles (Fe_3O_4@SiO_2@MOFs) for Removal of Congo Red and Methylene Blue from Water Solution", *J. Chem. Eng. Data*, **64**(6), pp. 2455–2463 (2019).
32. Abbas, M., "Fe_3O_4/SiO_2 Core/Shell Nanocubes: Novel Coating Approach with Tunable Silica Thickness and Enhancement in Stability and Biocompatibility", *J. Nanomed. Nanotechnol.*, **05**(06) (2014).
33. Nurdin Bukit, E. F., Simamora1, P., and Sinaga1, T., "Synthesis Of Fe_3O_4 Nanoparticles Of Iron Sand Coprecipitation Method With Polyethylene Glycol 6000", **7**(091207), pp. 110–115 (2015).
34. Li, Q., Kartikowati, C. W., Horie, S., et al., "Correlation between particle size/domain structure and magnetic properties of highly crystalline Fe3O4 nanoparticles", *Sci. Rep.*, **7**(1), pp. 1–4 (2017).
35. Prado, Y., Dia, N., Lisnard, L., et al., "Tuning the magnetic anisotropy in coordination nanoparticles: Random distribution versus core–shell architecture", *Chem. Commun.*, **48**(93), pp. 11455–11457 (2012).
36. Klokkenburg, M., Vonk, C., Claesson, E. M., et al., "Direct imaging of zero-field dipolar structures in colloidal dispersions of synthetic magnetite", *J. Am. Chem. Soc.*, **126**(51), pp. 16706–16707 (2004).
37. Salman, A. D., Juzsakova, T., Ákos, R., et al., "Synthesis and surface modification of magnetic Fe_3O_4@SiO_2 core-shell nanoparticles and its application in uptake of scandium (III) ions from aqueous media", *Environ. Sci. Pollut. Res.*, **28**(22), pp. 28428–28443 (2021).
38. Wan, D., Li, W., Wang, G., et al., "Size-controllable synthesis of Fe_3O_4 nanoparticles through oxidation-precipitation method as heterogeneous Fenton catalyst", *J. Mater. Res.*, **31**(17), pp. 2608–2616 (2016).
39. Dawn, R., Zzaman, M., Faizal, F., et al., "Origin of Magnetization in Silica-coated Fe_3O_4 Nanoparticles Revealed by Soft X-ray Magnetic Circular Dichroism", *Brazilian J. Phys.*, **52**(3) (2022).
40. Ma, J., Sun, N., Wang, C., et al., "Facile synthesis of novel Fe_3O_4@SiO_2@mSiO_2@TiO_2 core-shell microspheres with mesoporous structure and their photocatalytic performance", *J. Alloys*

Compd., **743**, pp. 456–463 (2018).
41. Bhaduri, K., Das, B. D., Kumar, R., et al., "Recyclable Au/SiO_2 -Shell/Fe_3O_4 -Core Catalyst for the Reduction of Nitro Aromatic Compounds in Aqueous Solution", *ACS Omega*, **4**(2), pp. 4071–4081 (2019).
42. Düsenberg, B., Singh, A. K., Schmidt, J., et al., "Spray agglomeration of polymer particles: Influence of spray parameters on shape factors", *Powder Technol.*, **422**, (2023).
43. Guan, H., Su, Q., Wang, R., et al., "Why can hybrid nanofluid improve thermal conductivity more? A molecular dynamics simulation", *J. Mol. Liq.*, **372**, p. 121178 (2023).
44. Hou, J., Shao, C., Huang, L., et al., "Why is the thermal conductivity of Janus nanofluid larger?–From the perspective of aggregation morphology", *Powder Technol.*, **430**(August), p. 119005 (2023).
45. Théodon, L., Debayle, J., and Coufort-Saudejaud, C., "Morphological characterization of aggregates and agglomerates by image analysis: A systematic literature review", *Powder Technol.*, **430**, p. 119033 (2023).

Figure 1. A Schematic illustration of the fabrication of a core-shell structure Fe_3O_4@SiO_2 NPs[10,15].

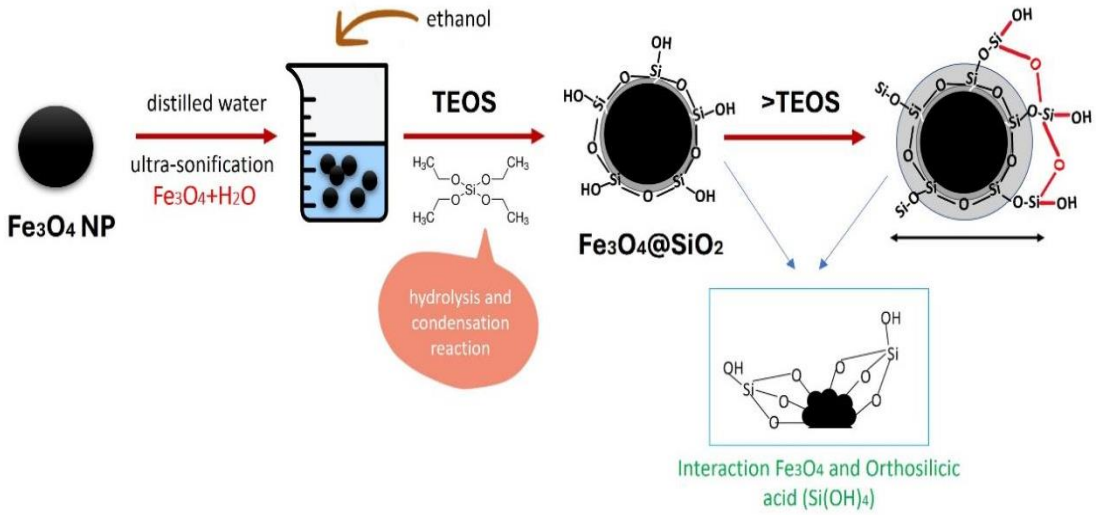

Figure 2. Pattern Diffraction of: (a) SiO_2, (b) Fe_3O_4, and (c-e) Fe_3O_4@SiO_2 core-shell: 45, 55, and 65

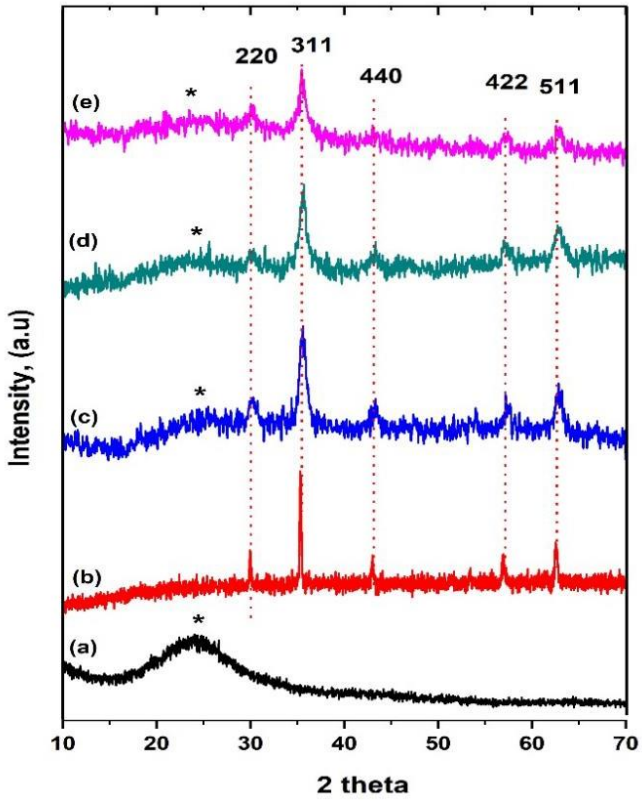

Figure 3. The infrared spectra of (a) Fe_3O_4, (b) SiO_2, and (c-d) Fe_3O_4@SiO_2 were synthesized by in-situ method with a ratio of TEOS 45 (c), 55 (d), and 65 (e).

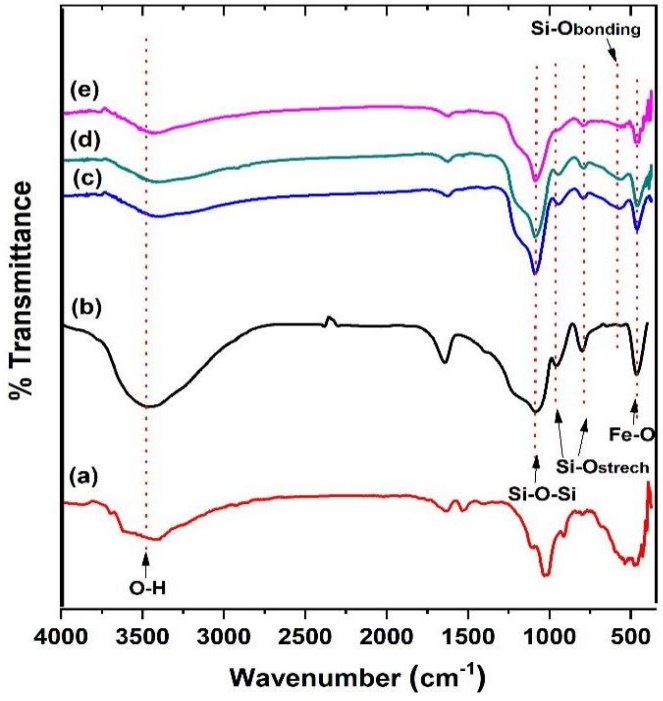

Figure 4. The coercivity field of (a) Fe_3O_4 (red line), (b)Fe_3O_4@SiO_2 with TEOS ratio 45 (black line), (c) TEOS ratio 55 (green line), and (d) TEOS ratio 65 (blue line)

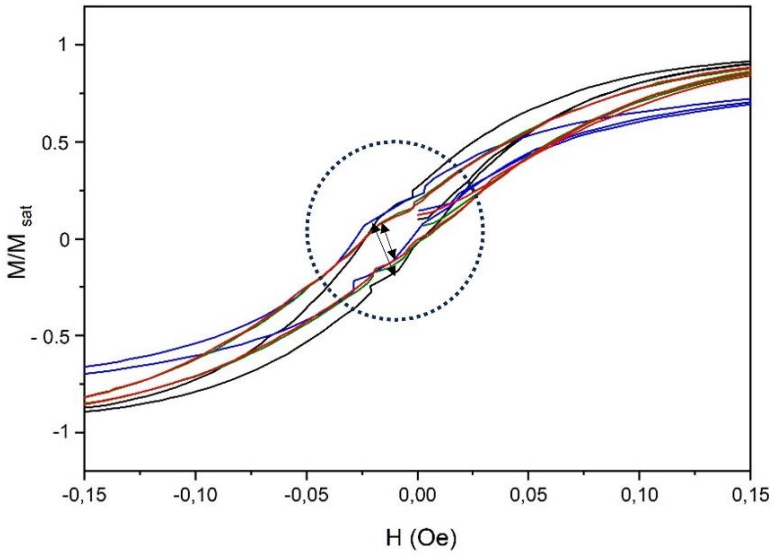

Figure 5. The curve of hysteresis of (a) Fe_3O_4 (red line), (b)Fe_3O_4@SiO_2 with TEOS ratio 45 (black line), (c) TEOS ratio 55 (green line), and (d) TEOS ratio 65 (blue line)

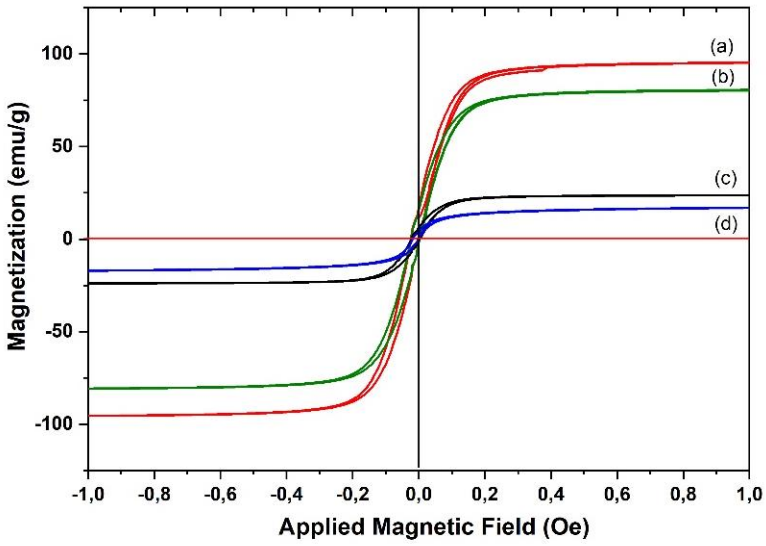

Figure 6. SEM Images of Fe_3O_4@SiO_2 core-shells, for TEOS ratio 45 (a) and 65 (b)

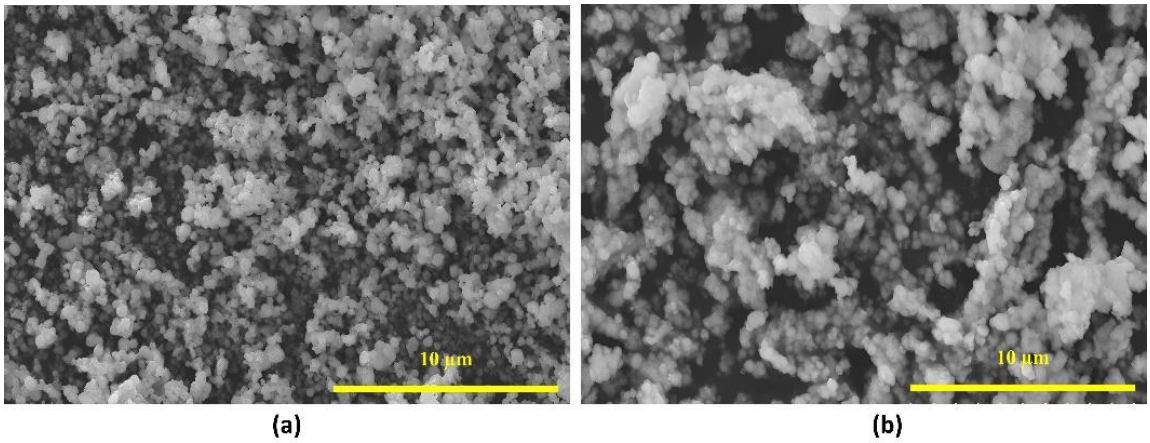

Figure 7. TEM images of Fe_3O_4 and Fe_3O_4@SiO_2 (core-shell): Fe_3O_4 particles (a-b) and SiO_2 shell thickness for core-shell with TEOS ratios of 45 (c) and 65 (d).

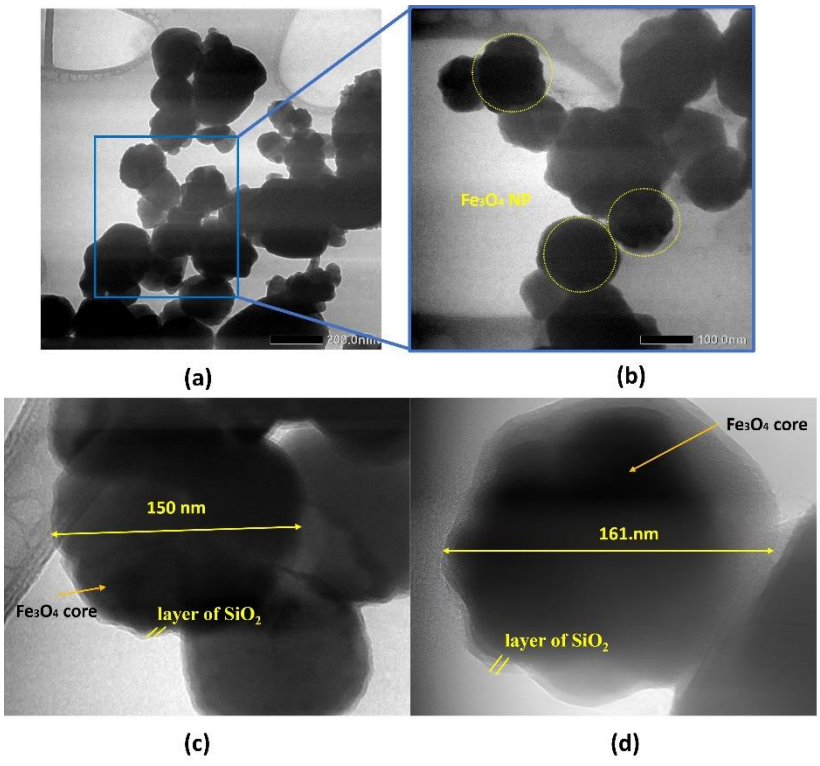

Figure 8. EDX Mapping of Fe_3O_4@SiO_2 core-shells nanoparticles with TEOS ratio: 45 (a) and 65 (b)

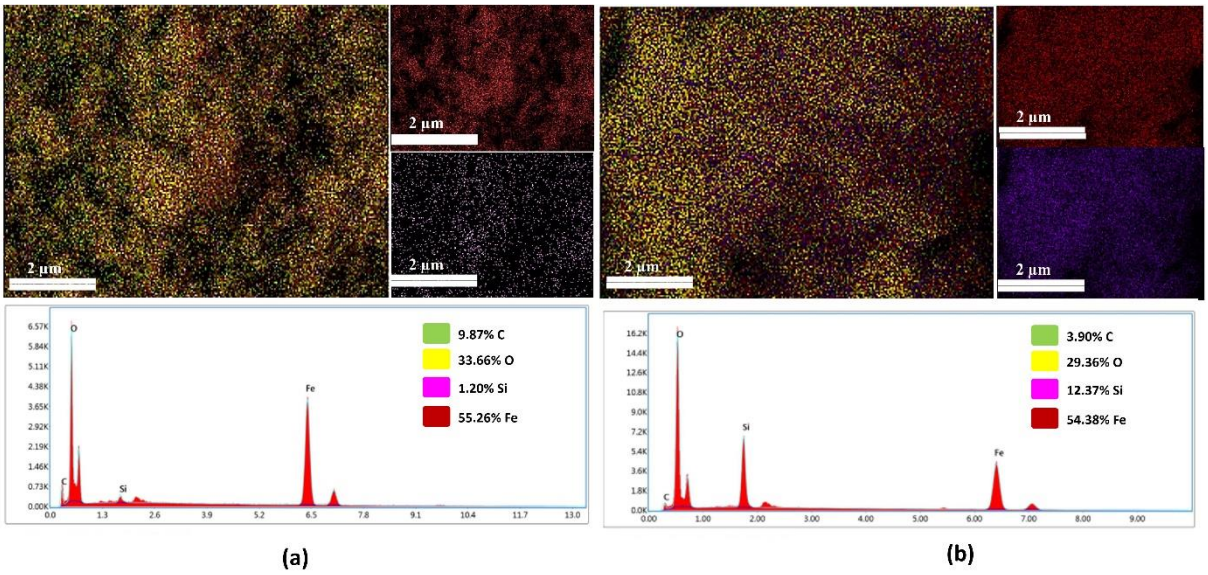

Figure 9. N_2 Adsorption-desorption of Fe_3O_4@SiO_2-core-shells ratio TEOS: (a) 45,(b) 55, and (c) 65

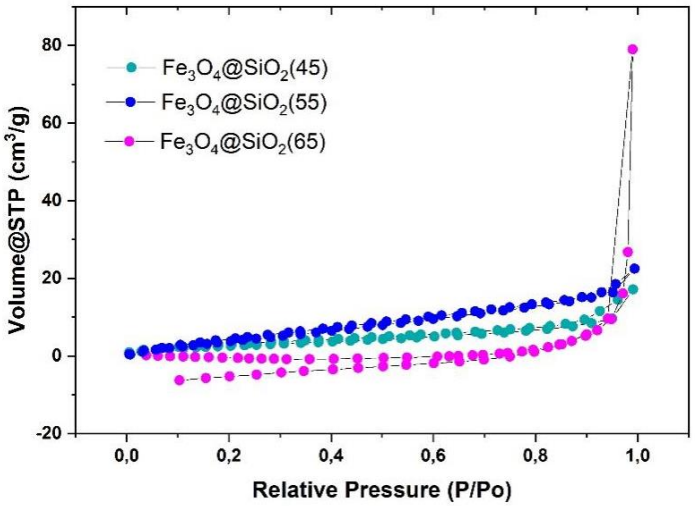

Figure 10. Pore size distribution by DFT method of Fe_3O_4@SiO_2-core-shells ratio TEOS: (a) 45, (b) 55, and (c) 65

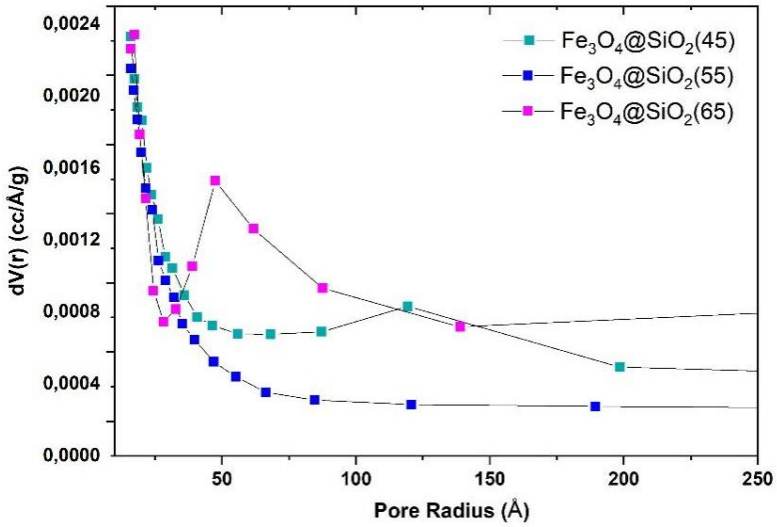

Table 1. Pattern X-ray of $Fe_3O_4@SiO_2$ core-shell nanoparticles

Peak *(2 theta), samples of Core@Shell (Fe_3O_4:SiO_2)*			*Crystal Field (hkl)*	*Average Crystallite Size (Debye Scharrer) (nm)* $\boldsymbol{D = (0.9\lambda/\beta\cos\theta)}$ *hkl (311)*			Ref
45	55	65					
29.98°	29.07°	30.01°	(220)				[19]
35.39°	35.34°	35.35°	(311)	8.47	14.12	22.59	[7]
43.02°	42.99°	43.00°	(400)				[30]
53.51°	53.44°	53.47°	(422)				[31]
56.96°	56.89°	56.95°	(511)				[29]
62.49°	62.46°	62.49°	(440)				[6] [32]

Table 2. Magnetic data of $Fe_3O_4@SiO_2$ core-shell nanoparticles by VSM

Sample	*Crystal Size (nm)*	*Ms (emu/g)*	*Hc (Tesla)*	*Mr (emu/g)*
Fe_3O_4	1.6	95.01	0.067	19.86
$Fe_3O_4@SiO_2(45)$	8.47	80.14	0.040	18.67
$Fe_3O_4@SiO_2(55)$	14.12	23.73	0.014	7.226
$Fe_3O_4@SiO_2(65)$	22.59	17.13	0.013	4.27

Table 3. Surface area, pore volume, and pore diameter of Fe_3O_4@SiO_2-core-shell nanoparticles

Materials	S_{BET} (m^2/g)	*Pore volume (cc/g)*	*Pore diameter (Å)*
Fe_3O_4@SiO_2(45)	10.50	0.02	27.69
Fe_3O_4@SiO_2(55)	21.04	0.03	33.04
Fe_3O_4@SiO_2(65)	80.23	0.83	88.17

Biographies:

Munasir Nasir received his PhD from the Institut Teknologi Sepuluh Nopember (ITS), Surabaya, Indonesia. He is a Professor and Head of Physics Department at Universitas Negeri Surabaya (Unesa), Indonesia. He has numerous publications (more than 50) in international conferences and journals with impact and patents. He is actively involved in studies of natural materials, nanomaterials, and their applications. Recently, He has developed materials for drug delivery systems, graphene-based membrane materials for desalination and filtration of water contaminated with pollutants, ZnO/rGO and TiO_2/rGO nanomaterials for photocatalysts, and ZnO as a quantum dot. His research interests include green synthesis of nanomaterials, materials for medicine, and materials for energy.

Ahmad Taufiq is a Professor and Head of Physics Department at Universitas Negeri Malang (UM), Indonesia. He is also a Vice President of Materials Research Society of Indonesia (MRS-id) and a Head of Scientific Committee of Indonesian Magnetic Society (IMS). His research interests include synthesis and characterization of nanomaterials for advanced applications. He has hundreds of published articles in reputable international journals with impact and dozens of patents. More than one hundred research grants were funded from the university and several national and international institutions. He also received several prestigious awards and most recently was named National Academic Leader in the Science Sector from the Indonesian Government at the end of 2023.

Nuhaa Faaizatunnisa received her B.S. degree in Chemistry from Sebelas Maret University (UNS) Surakarta, Indonesia, in 2019 and received an M.Sc. degree in Chemistry from Institut Teknologi Sepuluh Nopember (ITS) Surabaya, Indonesia in 2022. He is a doctoral candidate (Ph.D.) in Inorganic Chemistry at Sepuluh Nopember Institut Teknologi Sepuluh Nopember (ITS). His research interests focus on Metal-Organic Frameworks (MOFs), inorganic materials, photocatalysis, drug delivery systems, and adsorption.

Lydia Rohmawati received B.S. and M.Sc. degrees in Materials Physics from Institut Teknologi Sepuluh Nopember (ITS), Surabaya, Indonesia. She is working as an Assistant Professor at Department of Physics at Universitas Negeri Surabaya (Unesa). Her research interests focus on the fabrication and implementation of nanomaterials in the medical field, waste processing of organic dyes, sensors and materials energy.